Orientation control of $KNbO_3$ film grown on glass substrates by $Ca_2Nb_3O_{10}^-$ nanosheets seed layer

F. Baudouin , V. Demange , S. Ollivier , L. Rault , A.S. Brito , A.S. Maia , F. Gouttefangeas , V. Bouquet , S. Députier , B. Bérini , A. Fouchet , M. Guilloux-Viry

PII: S0040-6090(19)30709-6
DOI: https://doi.org/10.1016/j.tsf.2019.137682
Reference: TSF 137682

To appear in: *Thin Solid Films*

Received date: 24 June 2019
Revised date: 30 October 2019
Accepted date: 30 October 2019

Please cite this article as: F. Baudouin , V. Demange , S. Ollivier , L. Rault , A.S. Brito , A.S. Maia , F. Gouttefangeas , V. Bouquet , S. Députier , B. Bérini , A. Fouchet , M. Guilloux-Viry , Orientation control of $KNbO_3$ film grown on glass substrates by $Ca_2Nb_3O_{10}^-$ nanosheets seed layer, *Thin Solid Films* (2019), doi: https://doi.org/10.1016/j.tsf.2019.137682

Highlights

- $KNbO_3$ films grown on two-dimensional $Ca_2Nb_3O_{10}^-$ nanosheets covering glass substrate.
- (001) preferential orientation induced by subjacent nanosheets layer.
- Similar microstructure as epitaxial film grown on (100)$SrTiO_3$.

Orientation control of $KNbO_3$ film grown on glass substrates by $Ca_2Nb_3O_{10}^-$ nanosheets seed layer

F. Baudouin[a,*], V. Demange[a,c*], S. Ollivier[a], L. Rault[c], A. S. Brito[b], A. S. Maia[b], F. Gouttefangeas[c], V. Bouquet[a], S. Députier[a], B. Bérini[d], A. Fouchet[e], M. Guilloux-Viry[a,c]

[a]*Univ Rennes, CNRS, ISCR, 263, Avenue du Général Leclerc, F-35042 Rennes, France*

[b]*Laboratório de NPE-LACOM – Federal University of Paraíba, 58051-900, João Pessoa, PB, Brazil*

[c]*Univ Rennes, CNRS, ScanMAT - UMS 2001, 263, Avenue du Général Leclerc, F-35042 Rennes, France*

[d]*Groupe d'Etude de la Matière Condensée (GEMaC), Université de Versailles Saint-Quentin en Yvelines, Université Paris-Saclay CNRS, 45 avenue des Etats Unis, F-78035 Versailles, France*

[e] *NORMANDIE UNIV, ENSICAEN, UNICAEN, CNRS CRISMAT, 6 Boulevard du Maréchal Juin, F-14050 Caen, France*

Keywords: Inorganic nanosheets, Thin films, Langmuir-Blodgett, Pulsed laser deposition, Transmission electron microscopy

ABSTRACT

$KNbO_3$ films have been deposited by pulsed laser deposition on glass substrates covered by $Ca_2Nb_3O_{10}^-$ nanosheets used as seed layer, for the purpose of promoting (001) preferential orientation. Nanosheets have been prepared by the exfoliation process of $HCa_2Nb_3O_{10}$ phase that is obtained by cation exchange of the Dion-Jacobson $KCa_2Nb_3O_{10}$ phase in an acidic solution. Electron diffraction in transmission electron microscopy performed on $KCa_2Nb_3O_{10}$ and $HCa_2Nb_3O_{10}$ powders, and on $Ca_2Nb_3O_{10}^-$ nanosheets revealed formation of local superstructures that are not detected by X-ray diffraction due to the weakness of superstructure reflection intensities. Nanosheets were deposited on substrates using the Langmuir-Blodgett method. A smooth covering of the surface was shown by atomic force microscopy. 200 nm thick $KNbO_3$ films have been grown by pulsed laser deposition on $Ca_2Nb_3O_{10}^-$-NS/glass and on (001)$SrTiO_3$ substrates for comparison. Substrates covered with nanosheets induced highly textured (001)-oriented thin film, which possesses a similar microstructure as epitaxial film on single crystalline strontium titanate substrate.

1. Introduction

Downscaling in microelectronic undergoes certain limitations; therefore, solutions are required for the development and the integration of innovative properties (“More than Moore” concept) [1]. One of the solutions possible is to provide solutions for the growth of high quality complex oxides with multifunctional properties on low-cost substrates and for large surface electronic. The previously mentioned materials are often optimized by epitaxial growth on relatively expensive single-crystalline substrates, which offer a limited choice of materials and crystallographic orientations. Nanosheets (NS) are an eminent alternative to single-crystalline substrates; moreover they can be used as seed layers to induce epitaxy of complex oxides thin films. These NS are crystalline template of molecular thickness (oxide NS) with a lateral size that ranges between 100 nm and a few micrometers. In the past few years, various types of NS have been synthesized, including $Ti_{0.87}O_2^{0.52-}$ [2,3], $MnO_2^{0.4-}$ [4] or

$K_{0.8}Nb_6O_{17}^{3.2-}$ [5]. The NS used in this study are $Ca_2Nb_3O_{10}^-$ exfoliated from the layered perovskite Dion-Jacobson phase $KCa_2Nb_3O_{10}$ (KCN) [6,7]. Several oxide films ($LaNiO_3$, TiO_2, $Pr(Ca,Sr)TiO_3$, $Pb(Zr,Ti)O_3$, $SrTiO_3$ (STO), $CaBi_4Ti_4O_{15}$, $Na_{1-x}K_xNbO_3$) were grown with a preferential orientation on glass substrate by the use of $Ca_2Nb_3O_{10}^-$-NS as a seed layer [8–14]. The structure of KCN is monoclinic ($P2_1/m$, a = 7.741 Å, b = 7.707 Å, c = 14.859 Å, β = 97.51°, JCPDS card N°01-075-9853); furthermore, it could be described in a larger tetragonal cell with lattice constants a = 7.727 Å, b = 29.466 Å [6,15]. The structure consists of two-dimensional perovskite slabs interleaved with K^+ cations. The slabs are made of three NbO_6 corner-shared octahedra layers. After exfoliation, the NS have square lattice parameters a_{NS} = 3.854 Å that are similar to those of the perovskite type material such as $KNbO_3$ (KNO) (a_{pc} = 3.971 Å, b_{pc} = 4.027 Å, c_{pc} = 4.045 Å [16]). KNO is a ferroelectric material with moderate dielectrics permittivity values and high electro-optic coefficient, which could be promising for linear and non-linear optics [17,18]. Furthermore, this material possesses high piezoelectric and large electro-mecanic constants, which is interesting for acoustic waves applications [19]. In this study, KNO thin films were deposited by pulsed laser deposition (PLD) on glass recovered by $Ca_2Nb_3O_{10}^-$-NS, and on pristine single-crystalline (001)$SrTiO_3$ substrate for the purpose of comparison. Consequently, highly textured thin films have been obtained due to the low lattice mismatch between the NS lattice and KNO. This study demonstrates the possibility to integrate functional (001)-oriented KNO thin films of high quality on amorphous glass substrates using $Ca_2Nb_3O_{10}^-$-NS layer as a buffer template.

2. Experimental procedure

2.1. Synthesis and deposition of $Ca_2Nb_3O_{10}^-$ nanosheets on glass substrates

Powder of KCN oxide was synthesized by solid state reaction. K_2CO_3 (Acros Organics, 99 %), Ca_2CO_3 (R.P. Normapur, 99.5 %) and Nb_2O_5 (Alfa Aesar, 99.5 %) precursors were ball-

milled in ethanol for 5 h before a 10 hours thermal treatment at 1100°C. According to Ebina et al.'s method [20], the KCN oxide was then proton-exchanged in 6 M HNO_3 for 3 days. The protonated phase was exfoliated by its reaction with tetra(n-butyl)ammonium hydroxide (TBAOH) in a molar ratio 1:1, for 14 days. The obtained (TBA)$Ca_2Nb_3O_{10}$ NS were deposited on a low expansion fused silica (glass) substrates (OHARA, S-TIH-53, 10x10 mm^2) using Langmuir-Blodgett method with a KSV NIMA instrument, as stated by Dral *et al*. [21]. A heating treatment at 110°C and an UV treatment were carried out to stick NS at the substrate surface, by decomposing TBA^+ ions and evaporating water [22].

2.2. Elaboration of KNO thin films by PLD

The ceramic target was prepared using KNO powder synthesized by a solid-state reaction at 1000°C for 12 h in air using niobium oxide Nb_2O_5 (Alfa Aesar), hydrated potassium carbonate K_2CO_3 $1.5H_2O$ (Alfa Aesar) powders. The aforementioned components were mixed in a planetary ball mill for 25 min at 400 rotations per minutes speed (PM100, Retsch); subsequently, the powders were K-enriched with potassium nitrate KNO_3 powder (Prolabo), in order to balance the potassium loss during laser deposition due to the volatility of K_2O. Afterwards, the powders were uniaxially pressed into 25-mm-diameter targets and annealed at 500°C in air for 6 h. The KNO thin films were deposited by PLD technique on the glass substrates (surface: 10x10 mm^2, 2 mm thick) uncovered and covered by $Ca_2Nb_3O_{10}^-$-NS, and on 5x5 mm², 0.5 mm thick (001)STO (*Pm*-3*m*, *a* = 3.905 Å, JCPDS card N°01-073-0661, Crystal GmbH). Prior to KNO deposition, STO substrates were successively ultrasonically cleaned in acetone for 5 min and in isopropyl alcohol for 5 min. The KNO ceramic target was ablated with a KrF excimer laser (Coherent company, pulse duration 20 ns, λ = 248 nm) set at energy: 225 mJ, fluence: 2-3 $J.cm^{-2}$, and a 2 Hz frequency. The KNO films were grown at a substrate-target distance of 60 mm under 30 Pa oxygen partial pressure during a deposition

time of 15 min. Using a pyrometer, the temperature measured at the substrate surface was 550°C for deposition on STO and 600°C for film on glass.

2.3. Powders and thin films characterizations

X-ray diffraction (XRD) characterizations of powders and thin films were carried out using a θ–2θ Bragg-Brentano diffractometer (Bruker AXS D8 Advanced) working with a monochromatized Cu Kα1 radiation and equipped with a 1D detector (192 channels). Rocking curve was carried out on thin films using a four-circle texture diffractometer (Bruker AXS D8 Discover) operating with Cu Kα radiation in θ–2θ and ω-scan modes, and equipped with a 1D detector (192 channels). The surface morphology of the NS deposited on glass by Langmuir-Blodgett method was investigated by Atomic Force Microscopy (AFM) using a NT-MDT Ntegra instrument in tapping mode. Scanning electron microscopy (SEM) has been performed with a field emission gun Jeol JSM 7100 instrument working at 10 kV (for films grown on STO) and 5 kV (for films grown on glass), respectively. Compositional analysis were performed on carbon-coated powders with an energy dispersive X-ray spectroscopy detector coupled to the SEM (SEM-EDXS, SDD X-Max 50 mm^2, Oxford Instruments). Transmission electron microscopy (TEM) experiments were performed by using a LaB_6 Jeol 2100 instrument equipped with an Oxford Aztec 80 mm^2 SDD device for EDXS analysis (TEM-EDXS). Transmission electron bright field and electron diffraction patterns (EDPs) were recorded using a GATAN Orius SC200D charge coupled device camera. Powder samples for TEM were prepared by crushing the powder in a mortar in ethyl alcohol. A droplet of the obtained suspension was then put on an amorphous carbon copper grid (Agar). NS sample was prepared by dripping a droplet of the diluted colloidal suspensions on the same kind of grid.

3. Results and discussion

The XRD patterns of KCN and $HCa_2Nb_3O_{10}$ (HCN) powders are shown in Fig. 1. Pattern of KCN is indexed considering the previously mentioned monoclinic structure. The pattern of the protonated powder, after 72 h in acid, displays the peaks of the $HCN.1.5H_2O$ phase (a = 3.854 Å, c = 16.225 Å, Joint Commitee on Powder Diffraction Standards (JCPDS) card No. 00-39-0915) [23]). Compared to the parent phase, the (00l) peaks of HCN are shifted toward higher angles, due to the increase of the interlamellar space induced by the K^+ exchange by H^+ ions and the insertion of water (H_3O^+), from $d^{KCN}(002)$ = 14.73 Å to $d^{HCN.1.5}(001)$ = 16.22 Å.

After drying the powder at 80°C for 2 hours, two dehydrated phases are obtained, namely $HCN.0.5H_2O$ (a = 5.452 Å, c = 14.414 Å, *P4/mbm*, JCPDS card No. 01-077-4249, interlamellar space $d^{HCN.0.5}(001)$ = 14.41 Å [23,24]) with an intermediately hydrated phase, $HCN.xH_2O$ (interlamellar space $d^{HCN.x}(001)$ = 15.14 Å) that corresponds to the insertion of approximatively one molecule of water. Indeed, the insertion of water molecules inside the lamellar compound induces shift of perovskite sheets that involves changes of coordinence for the molecules and modifying the value of the lattice constant c. Interestingly, the dehydration and hydration phenomena are perfectly reversible; the dehydrated powder was set under a moist atmosphere in an oven; consequently, the peaks shift again to a lower angle as displayed on Fig. 1. This phenomena is similar to the one observed by Jacobson *et al*. [23].

TEM electron diffraction were performed on KCN and HCN powders, and on NS. Fig. 2a shows the [001] zone axis selected-area EDPs of two crystals of KCN, which correspond to the normal of the NS surface. In the first EDP, the {h00} and {0k0} reflections, h, k odd, (labeled by arrows in the figure), are present with a weak intensity as expected for the monoclinic structure [15]. In the second EDP (see Fig. 2b), these reflections are absent indicating a change of octahedral tilt for some crystals, which results in either a large (a ~ 7.8 Å, with extinctions) or in a smaller (a ~ 3.9 Å) tetragonal cell. Composition of KCN powder

was found to be around $K_{1.1\pm0.1}Ca_{2.1\pm0.2}Nb_{3\pm0.3}O_x$ by TEM-EDXS and SEM-EDXS analysis. For the protonated phase, four different patterns along the [001] zone axis were recorded (Fig. 2c-f). In Fig. 2c, the presence of weak superlattice reflections at {½, 0, 0} and {0, ½, 0} positions (labeled by arrows in the figure) indicate that the lattice constants *a* and *b* are actually double that was that determined by XRD. The fact that these reflections are detected only by electron diffraction and not by XRD was already reported by Jacobson *et al*. [23]. In Fig. 2d, the EDP is different with the presence of weak reflections at {½, ½, 0} positions (labeled by an arrow in the figure), but no longer along *a** and *b** axes. In both cases, these superlattice reflections result from the tilting of NbO_6 octahedra along [100], [010] and [001] axis [23,25]. EDPs in Fig. 2e-f display two other superstructures with five extra reflections along the [210]* direction, and twenty-five extra reflections along the [430]* direction (labeled by arrows in the figure); these reflections correspond to lattice distances of about 8.6 Å and 19.3 Å, respectively. These particular superstructures can arise from octahedral tilts or oxygen vacancies ordering. Composition of HCN powder was found to be around $K_{0.15\pm0.1}Ca_{2.1\pm0.2}Nb_{3\pm0.3}O_x$ by TEM-EDXS and SEM-EDXS analysis showing therefore that a slight amount of potassium is still present in the exchanged phase, as previously observed [26,27].

Fig. 2g shows a brighfield TEM micrograph of several NS collected from the NS colloid, showing the different dimensions (from about 0.1 µm to 5 µm) obtained after the exfoliation process. Fig. 2h is a [001] zone axis EDP of a single NS. Comparison between brightfield micrographs and EDP shows that the [100]* and [010]* directions are parallel to the NS edges. In addition to the fundamental reflections (corresponding to lattice parameters $a \sim b \sim$ 3.88 Å), all the recorded EDPs on NS exhibit very weak superlattice {½, ½, 0} reflections, due to a tilting of octahedra, indicating that a $\sqrt{2}a$ lattice constant should be used to describe the tetragonal lattice [25]. Composition of NS was found to be $Ca_{2.4\pm0.7}Nb_{3\pm0.7}O_x$ by TEM-

EDXS. Fig. 3 displays the AFM micrograph of the NS seed layer deposited on the glass by Langmuir-Blodgett method. It shows that the substrate surface is covered by a smooth and almost continuous monolayer of NS. The NS thickness is around 2 nm, in agreement with previous studies [3,28]. Among the literature, thickness of $Ca_2Nb_3O_{10}^-$ NS is found to be between 1.4 to 3.0 nm [29,30], due to the intercalation of water and organic TBA^+ residues between the substrate and the NS.

XRD patterns of KNO thin films deposited by PLD on (001)STO, on glass and $Ca_2Nb_3O_{10}^-$-NS/glass substrates are shown in Fig. 4. The KNO film is poorly crystallized on uncovered glass (the intensity was multiply by 50 in order to enhance the signal on noise) and the diagram presents (001) and (110) reflections. In the two other cases, only $\{h00\}_{pc}$ peaks are observed, indicating preferential orientation growth of the niobate films, and demonstrating that the monolayer film of NS induced on glass this oriented growth. The lattice mismatch for (001) oriented growth of KNO on $Ca_2Nb_3O_{10}^-$ NS is -2.6 %, and -1.7 % on (001)STO. The film on STO is obtained at a surface substrate temperature of 550°C. Pure KNO films are obtained on $Ca_2Nb_3O_{10}^-$-NS/glass at a surface substrate temperature of 600°C. Note that this temperature corresponds actually to a higher holder temperature than for the film deposited on STO. This difference is mainly due to the much higher thickness of the glass substrate. At higher temperature than 650°C, the film presents a secondary phase in addition to KNO. TEM-EDXS analyses showed that it contains K, Nb, Na, Ba and O elements, indicating a diffusion of elements from the glass substrate (of composition approximatively $Si_{19.7}Na_{14.2}Ba_9Nb_6O_{51}$) through the film at this temperature. The rocking curves (ω-scan) displayed in Fig. 4 show low mosaicity of KNO on STO with the full-width-at-half-maximum value $\Delta\omega = 0.7°$ and a slightly higher mosaicity of KNO on $Ca_2Nb_3O_{10}^-$-NS/glass with $\Delta\omega = 2.1°$, indicating that the crystallites are less aligned on the later. The Rq root mean square (RMS) roughness obtained from $5 \times 5\ \mu m^2$ AFM images (Fig. 3) increases from 0.4 ± 0.1 nm

for the glass substrate up to 0.66 ± 0.2 nm for the NS/glass substrate. The Rq value of STO is 0.08 ± 0.05 nm. After deposition, the Rq value of KNO/NS/glass is 2.2 ± 0.2 nm while that of KNO/STO is 1.85 ± 0.2 nm. Therefore the significant difference in roughness between both substrates does not involve an important difference in roughness between the KNO films. For the NS coated glass substrates, the films cover the NS and the interstices. The films morphology was investigated by in-plane-view and cross-sectional SEM as shown in Fig. 5. The film deposited on (001)STO shows a dense array of epitaxied square-shaped KNO crystals with lateral size lying between 50 and 230 nm, while the film deposited on $Ca_2Nb_3O_{10}^-$-NS/glass shows a textured growth. This film is also made of square-shaped crystals of the same size. This shape is characteristic of (001)-oriented KNO grains [31]. It appears that the surface morphology of the KNO film was influenced by the underlying NS, and that the grains grown on the same NS present an identical in-plane orientation. Control of crystallographic orientation of KNO film on glass by NS is therefore realized. Cross-sectional view (inset in Fig. 5b) indicates that the thickness of the thin film is homogeneous and about 200 nm.

4. Conclusions

Inorganic $Ca_2Nb_3O_{10}^-$ nanosheets have been synthesized from exfoliation of layered proton-exchanged $HCa_2Nb_3O_{10}$ phase. Electron diffraction experiments have shown the formation of unseen superstructures in the parent phase, the protonated oxide and the nanosheets. Highly-textured (001) $KNbO_3$ film have been grown on glass using inorganic $Ca_2Nb_3O_{10}^-$ nanosheet as seed layer. The importance of the growth temperature was also investigated. If the growth temperature is higher than 650°C, a diffusion of the element of the substrate was found in the film, showing the importance of limiting the growth temperature and to know the composition of the substrate. For lower temperature, around 600°C, the films were found to have a high

crystalline quality similarly to the films epitaxially grown on single crystalline (001)$SrTiO_3$. Therefore, this method allows the growth of oriented ferroelectric $KNbO_3$ films on low-cost substrate.

Declaration of interests

☒ The authors declare that they have no known competing financial interests or personal relationships that could have appeared to influence the work reported in this paper.

Acknowledgements

SEM and TEM were performed on ScanMAT facilities platforms (UMS 2001, University of Rennes 1-CNRS). ISCR and ScanMAT received a financial support from the Région Bretagne, Rennes Métropole, the Département d'Ille et Vilaine and the European Union (CPER-FEDER 2007–2014, Présage Nos. 39126 and 37339, and CPER 2015-2020 MULTIMAT ScanMAT). The authors thank the French "Agence Nationale de la Recherche" (ANR) in the framework of the PolyNash project (ANR-17-CE08-0012).

Declaration of interest

None

References

[1] G.Q. Zhang, A.J. van Roosmalen, eds., More than Moore: creating high value micro/nanoelectronics systems, Springer, Dordrecht ; New York, 2009.

[2] H. Yuan, R. Lubbers, R. Besselink, M. Nijland, J.E. ten Elshof, Improved Langmuir-Blodgett Titanate Films via in Situ Exfoliation Study and Optimization of Deposition

Parameters, ACS Appl. Mater. Interfaces. 6 (2014) 8567–8574. doi:10.1021/am501380d.

[3] M. Osada, T. Sasaki, Exfoliated oxide nanosheets: new solution to nanoelectronics, J. Mater. Chem. 19 (2009) 2503–2511. doi:10.1039/b820160a.

[4] Z.H. Liu, K. Ooi, H. Kanoh, W.P. Tang, T. Tomida, Swelling and delamination behaviors of birnessite-type manganese oxide by intercalation of tetraalkylammonium ions, Langmuir. 16 (2000) 4154–4164. Doi:10.1021/la9913755

[5] G.B. Saupe, C.C. Waraksa, H.-N. Kim, Y.J. Han, D.M. Kaschak, D.M. Skinner, T.E. Mallouk, Nanoscale Tubules Formed by Exfoliation of Potassium Hexaniobate, Chem. Mater. 12 (2000) 1556–1562. doi:10.1021/cm981136n.

[6] M. Dion, M. Ganne, M. Tournoux, Nouvelles familles de phases MIMII2Nb3O10 a feuillets “perovskites,” Mater. Res. Bull. 16 (1981) 1429–1435. doi:10.1016/0025-5408(81)90063-5.

[7] A.J. Jacobson, J.W. Johnson, J.T. Lewandowski, Interlayer chemistry between thick transition-metal oxide layers: synthesis and intercalation reactions of K[Ca2Nan-3NbnO3n+1] (3 .ltoreq. n .ltoreq. 7), Inorg. Chem. 24 (1985) 3727–3729. doi:10.1021/ic00217a006.

[8] K. Kikuta, K. Noda, S. Okumura, T. Yamaguchi, S. Hirano, Orientation control of perovskite thin films on glass substrates by the application of a seed layer prepared from oxide nanosheets, J. Sol-Gel Sci. Technol. 42 (2007) 381–387. doi:10.1007/s10971-006-0200-z.

[9] T. Shibata, K. Fukuda, Y. Ebina, T. Kogure, T. Sasaki, One-nanometer-thick seed layer of unilamellar nanosheets promotes oriented growth of oxide crystal films, Adv. Mater. 20 (2008) 231-235. doi:10.1002/adma.200701381.

[10] H. Tetsuka, H. Takashima, K. Ikegami, H. Nanjo, T. Ebina, F. Mizukami, Nanosheet Seed-Layer Assists Oriented Growth of Highly Luminescent Perovskite Films, Chem. Mater. 21 (2009) 21–26. doi:10.1021/cm8027912.

[11] T. Shibata, H. Takano, Y. Ebina, D.S. Kim, T.C. Ozawa, K. Akatsuka, T. Ohnishi, K. Takada, T. Kogure, T. Sasaki, Versatile van der Waals epitaxy-like growth of crystal films using two-dimensional nanosheets as a seed layer: orientation tuning of SrTiO3 films along three important axes on glass substrates, J. Mater. Chem. C. 2 (2014) 441–449. doi:10.1039/c3tc31787k.

[12] J. Kimura, I. Takuwa, M. Matsushima, T. Shimizu, H. Uchida, T. Kiguchi, T. Shiraishi, T.J. Konno, T. Shibata, M. Osada, T. Sasaki, H. Funakubo, Thermally stable dielectric responses in uniaxially (001)-oriented CaBi4Ti4O15 nanofilms grown on a Ca2Nb3O10-nanosheet seed layer, Sci. Rep. 6 (2016) 20713. doi:10.1038/srep20713.

[13] M.D. Nguyen, E.P. Houwman, G. Rijnders, Large piezoelectric strain with ultra-low strain hysteresis in highly c-axis oriented Pb(Zr0.52Ti0.48)O-3 films with columnar growth on amorphous glass substrates, Sci. Rep. 7 (2017) 12915. doi:10.1038/s41598-017-13425-w.

[14] S.H. Kweon, J.H. Kim, M. Im, W.H. Lee, S. Nahm. Physical Properties of (Na1−xKx)NbO3 Thin Film Grown at Low Temperature Using Two-Dimensional Ca2Nb3O10 Nanosheet Seed Layer, ACS Appl. Mater. Inter. 10 (2018) 25536-25546. DOI: 10.1021/acsami.8b09482

[15] T. Tokumitsu, K. Toda, T. Aoyagi, D. Sakuraba, K. Uematsu, M. Sato, Powder neutron diffraction study of layered perovskite, KCa2Nb3O10, J. Ceram. Soc. Jpn. 114 (2006) 795–797. doi:10.2109/jcersj.114.795.

[16] L. Katz, H.D. Megaw, The structure of potassium niobate at room temperature: the solution of a pseudosymmetric structure by Fourier methods, Acta Crystallogr. 22 (1967) 639–648. doi:10.1107/S0365110X6700129X.

[17] B.T. Matthias, J.P. Remeika, Dielectric Properties of Sodium and Potassium Niobates, Phys. Rev. 82 (1951) 727–729. doi:10.1103/PhysRev.82.727.

[18] G. Shirane, H. Danner, A. Pavlovic, R. Pepinsky, Phase Transitions in Ferroelectric KNb O 3, Phys. Rev. 93 (1954) 672–673. doi:10.1103/PhysRev.93.672.

[19] K. Nakamura, Y. Kawamura, Orientation dependence of electromechanical coupling factors in KNbO/sub 3/, IEEE Trans. Ultrason. Ferroelectr. Freq. Control. 47 (2000) 750–755. doi:10.1109/58.842064.

[20] Y. Ebina, K. Akatsuka, K. Fukuda, T. Sasaki, Synthesis and In Situ X-ray Diffraction Characterization of Two-Dimensional Perovskite-Type Oxide Colloids with a Controlled Molecular Thickness, Chem. Mater. 24 (2012) 4201–4208. doi:10.1021/cm302480h.

[21] A.P. Dral, D. Dubbink, M. Nijland, J.E. ten Elshof, G. Rijnders, G. Koster, Atomically Defined Templates for Epitaxial Growth of Complex Oxide Thin Films, J. Vis. Exp. 94 (2014) e52209. doi:10.3791/52209.

[22] B.-W. Li, M. Osada, T.C. Ozawa, Y. Ebina, K. Akatsuka, R. Ma, H. Funakubo, T. Sasaki, Engineered Interfaces of Artificial Perovskite Oxide Superlattices *via* Nanosheet Deposition Process, ACS Nano. 4 (2010) 6673–6680. doi:10.1021/nn102144s.

[23] A.J. Jacobson, J.T. Lewandowski, J.W. Johnson, Ion exchange of the layered perovskite KCa2Nb3O10 by protons, J. Common Met. 116 (1986) 137–146. doi:10.1016/0022-5088(86)90224-9.

[24] Y. Chen, X. Zhao, H. Ma, S. Ma, G. Huang, Y. Makita, X. Bai, X. Yang, Structure and dehydration of layered perovskite niobate with bilayer hydrates prepared by

exfoliation/self-assembly process, J. Solid State Chem. 181 (2008) 1684–1694. doi:10.1016/j.jssc.2008.06.014.

[25] F.F. Xu, Y. Bando, Y. Ebina, T. Sasaki, Modification of crystal structures in perovskite-type niobate nanosheets, Philos. Mag. A 82 (2002) 2655–2663. doi:10.1080/01418610210155771.

[26] T. Nakato, K. Ito, K. Kuroda, C. Kato, Photochemical behavior of perovskite-related layered niobates HA2Nb3O10 (A = Ca, Sr) intercalated with methylviologen, Microporous Mater. 1 (1993) 283–286. doi:10.1016/0927-6513(93)80071-2.

[27] Y. Song, N. Iyi, T. Hoshide, T.C. Ozawa, Y. Ebina, R. Ma, N. Miyamoto, T. Sasaki, Accordion-like swelling of layered perovskite crystals via massive permeation of aqueous solutions into 2D oxide galleries, Chem. Commun. 51 (2015) 17068–17071. doi:10.1039/c5cc05408g.

[28] K. Akatsuka, G. Takanashi, Y. Ebina, M. Haga, T. Sasaki, Electronic Band Structure of Exfoliated Titanium- and/or Niobium-Based Oxide Nanosheets Probed by Electrochemical and Photoelectrochemical Measurements, J. Phys. Chem. C. 116 (2012) 12426–12433. doi:10.1021/jp302417a.

[29] C. Wang, M. Osada, Y. Ebina, B.-W. Li, K. Akatsuka, K. Fukuda, W. Sugimoto, R. Ma, T. Sasaki, All-Nanosheet Ultrathin Capacitors Assembled Layer-by-Layer via Solution-Based Processes, Acs Nano. 8 (2014) 2658–2666. doi:10.1021/nn406367p.

[30] K.S. Virdi, Y. Kauffmann, C. Ziegler, P. Ganter, P. Blaha, B.V. Lotsch, W.D. Kaplan, C. Scheu, Band Gap Extraction from Individual Two-Dimensional Perovskite Nanosheets Using Valence Electron Energy Loss Spectroscopy, J. Phys. Chem. C. 120 (2016) 11170–11179. doi:10.1021/acs.jpcc.6b00142.

[31] A. Rousseau, V. Laur, M. Guilloux-Viry, G. Tanné, F. Huret, S. Députier, A. Perrin, F. Lalu, P. Laurent, Pulsed laser deposited KNbO3 thin films for applications in high frequency range, Thin Solid Films. 515 (2006) 2353–2360. doi:http://dx.doi.org/10.1016/j.tsf.2006.04.010.

List of figures

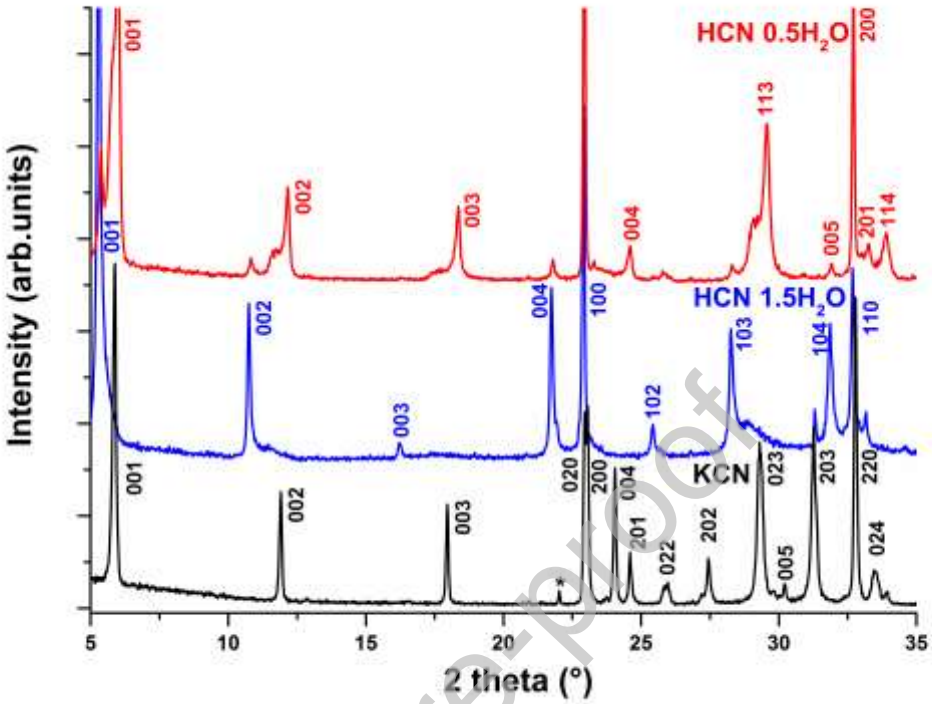

Fig. 1. a) XRD powder pattern of the KCN phase (*: KNO phase). b) XRD powder pattern of the HCN $1.5H_2O$ (HCN1.5) phase. c) XRD powder pattern of HCN1.5 after a few hours in a dry atmosphere corresponding to the HCN $0.5H_2O$ phase.

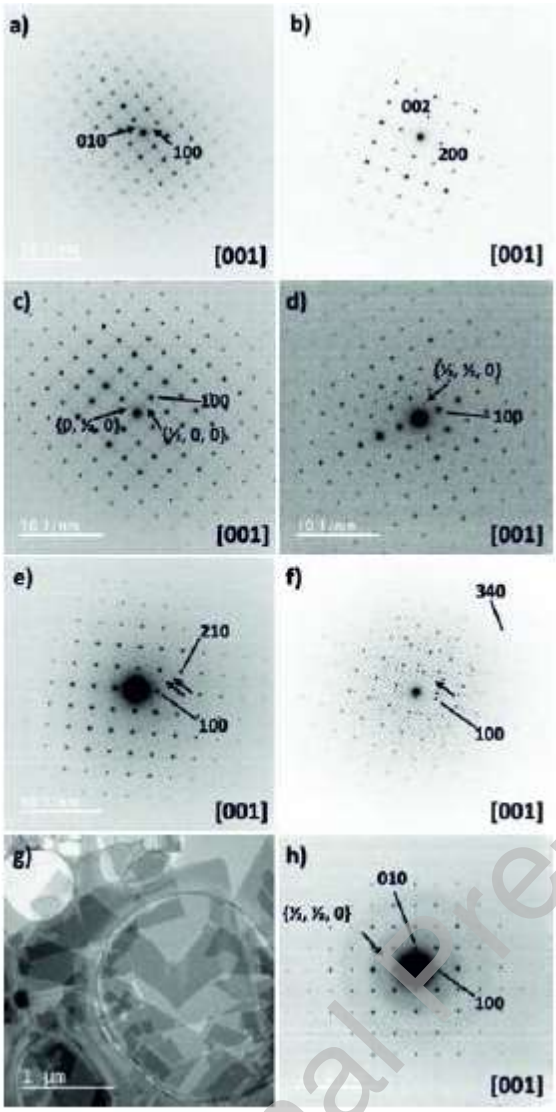

Fig. 2. a) EDP along the [001] zone axis of the monoclinic KCN phase. b) EDP of the KCN phase along the [001] zone axis showing weak superlattice reflections indicated by the arrows. c) EDP of the HCN $1.5H_2O$ phase showing weak superlattice reflections indicated by the arrows. d) EDP of the HCN $0.5H_2O$ phase showing weak reflections that should be forbidden, indicated by the arrows. e) EDP of the HCN $1.5H_2O$ phase showing weak superlattice reflections indicated by the arrows. These reflections are aligned along the (210) row. f) EDP of the HCN $1.5H_2O$ phase showing weak superlattice reflections indicated by the arrows. These reflections are aligned along the (430) row. g) Brightfield micrograph of the $Ca_2Nb_3O_{10}^-$-NS. h) EDP of a single $Ca_2Nb_3O_{10}^-$-NS. Weak reflections are indicated by the arrows.

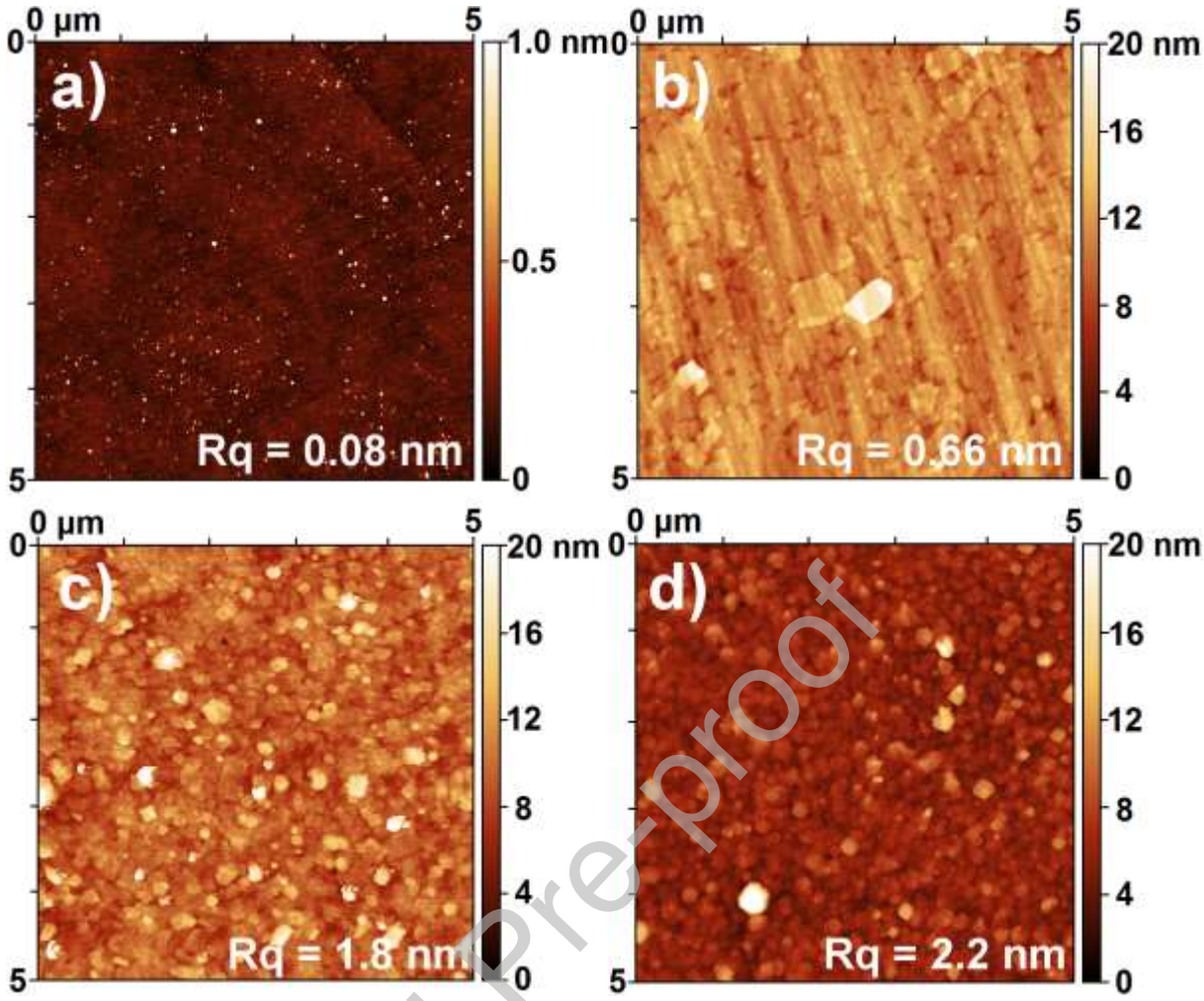

Fig. 3. AFM images of a) the STO substrate, b) the monolayer film of $Ca_2Nb_3O_{10}^-$-NS deposited on glass by Langmuir-Blodgett method, c) the KNO/STO film, d) the KN/$Ca_2Nb_3O_{10}^-$-NS/glass film.

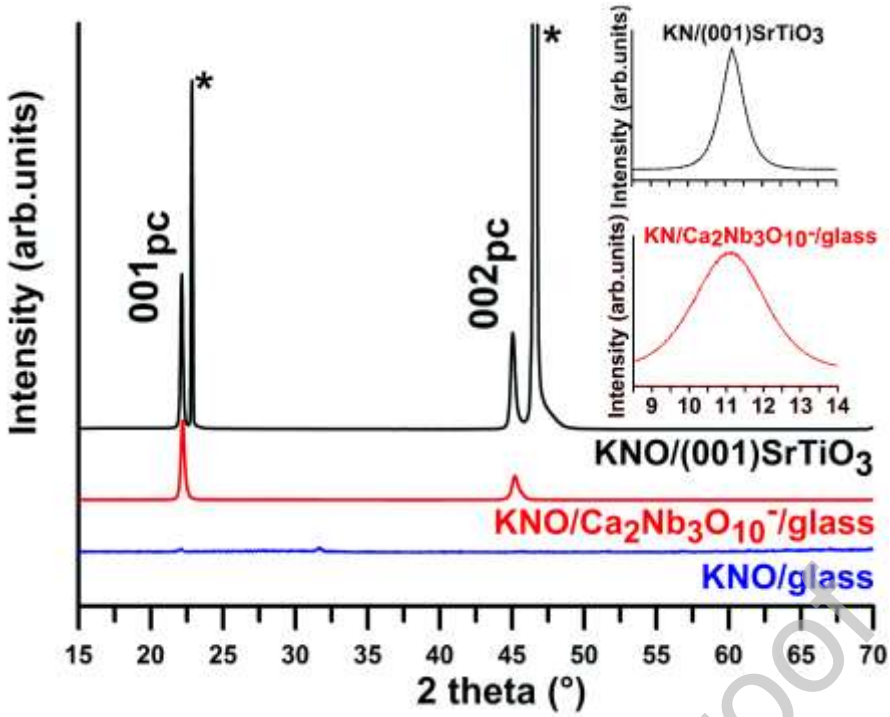

Fig. 4. θ/2θ XRD patterns of KNO thin films deposited on (100)STO at 550°C (black), on glass at 600°C (blue, the intensity was multiply by 50 to enhanced the signal display), $Ca_2Nb_3O_{10}^-$-NS/glass at 600°C (red) (*: STO). Insets: corresponding (001) KNO reflection rocking-curves.

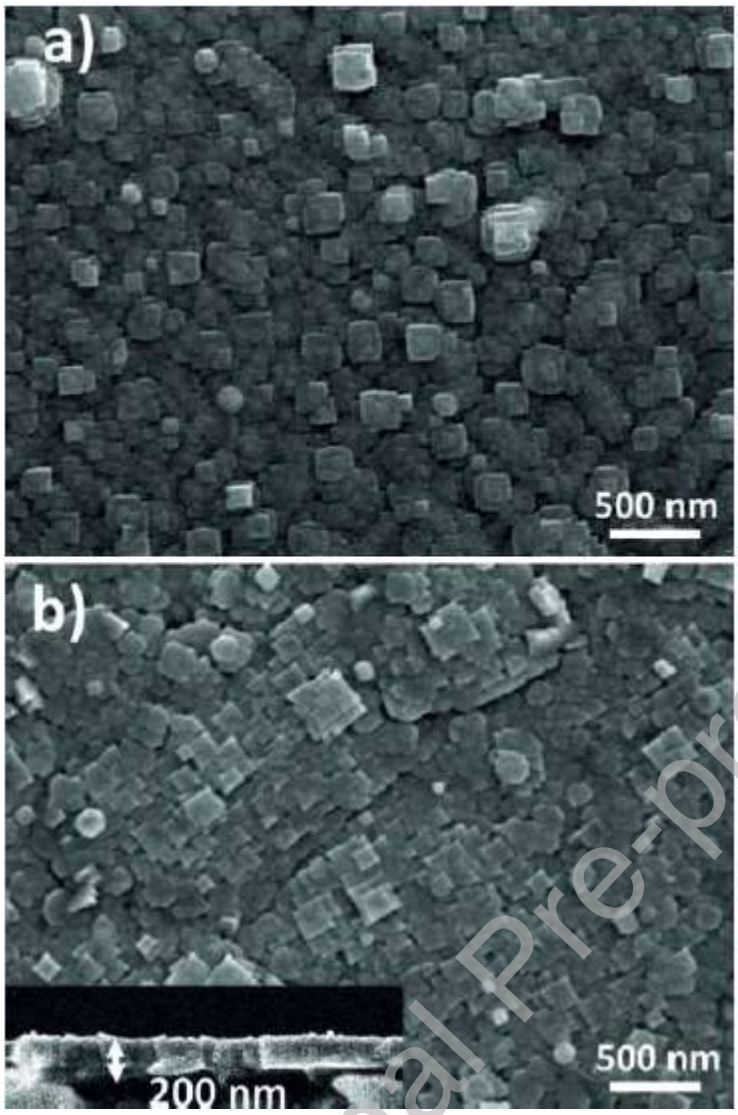

Fig. 5. Scanning electron micrographs of KNO thin films deposited on (100)STO at 550°C (a) and on $Ca_2Nb_3O_{10}^-$-NS/glass at 600°C. (b). Inset: cross-sectional view of the KNO film on $Ca_2Nb_3O_{10}^-$-NS/glass, showing the 200 nm thick film.